

13 **Abstract**

14 The year 2018 was one of the hottest and driest years in Europe having a large impact on
15 agriculture, ecosystems and society. The associated drought in central and northern Europe
16 underpins the need for water resources predictions at the seasonal to interannual time scale. In
17 this study, we propose a probabilistic, terrestrial prediction system including water resources
18 utilizing the Terrestrial Systems Modeling Platform, TSMP. Based on an existing climatology
19 from 1996 to 2018, a probabilistic prediction for the water year 2018/19 was performed
20 accounting for atmospheric uncertainty in an ensemble approach. The results show that the water
21 year 2017/18 is an outlier with respect to dry conditions considering all available years of the
22 climatology. The prediction shows that, on average, the water deficit will not be alleviated until
23 the end of 2019 and that there is a higher probability for anomalously dry conditions. However,
24 the current trajectory obtained from a simulation applying recent atmospheric reanalysis data is
25 located in the dry tail of the ensemble potentially indicating a continuation of a severe drought in
26 future.

27 **1 Introduction**

28 At the seasonal time scale and beyond, droughts associated with heat waves are difficult to
29 predict, mainly because of uncertainty related to the atmospheric forcing (Miralles et al., 2019).
30 However, the hypothesis is that memory effects related to slow dynamics of the groundwater-soil
31 water-vegetation (GSV) system render the prediction challenge an initial value problem, which
32 may lead to predictive skill potentially over extended periods (Dirmeyer, 2000). Here, the major
33 assumption is that memory effects including interactions of the GSV system with the
34 atmospheric forcing are correctly simulated in the forward model.

35 In recent years there have been many efforts to establish a reliable seasonal forecasting system
36 applying various approaches. First, there is the possibility of using statistical tools e.g. linear
37 stochastic models (e.g. Mishra and Desai, 2005), Bayesian frameworks (e.g. Madadgar and
38 Moradkhani, 2013) or the collection and transformation of multiple datasets (e.g. Hao et al.,
39 2015). These approaches rely on drought indices derived from as much observational data as
40 possible to derive probability density functions. Then there is the possibility to use climate
41 models with a dynamical core, e.g. Yuan et al. (2013) and Yuan and Wood (2013). Because
42 predictions with climate models alone generally do not lead to satisfactory results, there are
43 recent studies that combine models with observational data using machine learning methods
44 (Rhee and Im, 2017; Hosseini-Moghari and Araghinejad, 2015). Furthermore, there has been
45 success with an experimental combination of hydrological modeling and regional climate
46 forecasts in the Sub-Saharan region (Sheffield et al., 2013).

47 The importance of soil moisture and groundwater in the occurrence of extreme temperature
48 events and droughts has been shown previously (e.g., Seneviratne et al., 2010; Hirschi et al.,

49 2011). However, at the continental scale, weather forecast or climate models do not provide the
50 whole water cycle and strongly simplify the GVS system generally neglecting groundwater
51 dynamics. While hydrological models seem an alternative, at the continental scale, the
52 groundwater compartment and coupling with the soil water are also simplified (Zink et al.,
53 2016), which may affect adversely the simulation of memory effects (Lo & Famiglietti, 2010).
54 Additionally, in hydrologic modeling, potential impacts of the subsurface and land surface on
55 atmospheric processes affecting precipitation are not taken into account.

56 Thus, in order to relax simplifying assumptions, we propose the application of an integrated
57 terrestrial systems modeling approach for water resources and drought prediction. In this study,
58 integrated terrestrial modeling refers to the representation of the complete terrestrial hydrologic
59 and energy cycle from groundwater across the land surface into the atmosphere. In the recent
60 past, considerable advancements have been achieved since the early work of e.g., York et al.
61 (2002) and Maxwell et al. (2007) to couple subsurface, land surface and atmospheric models to
62 close the terrestrial cycles in models and provide physically consistent states and fluxes
63 throughout the terrestrial system. At the continental scale, which is of interest in this study, e.g.
64 Miguez-Macho and Fan (2012) and Walco et al. (2000) applied groundwater parameterizations
65 and simulated the terrestrial cycle over the Amazon and also globally at relatively coarse spatial
66 resolutions. Keune et al. (2016) used the Terrestrial Systems Modeling Platform (TSMP)
67 including a 3D variably saturated groundwater representation in a continuum approach to show
68 that surface-atmosphere feedbacks are well-captured and that groundwater actually mitigated the
69 2003 heatwave over Europe. Later Keune et al. (2018) showed that human water use related to
70 groundwater abstraction and irrigation may systematically change the distribution of water
71 resources due to local and non-local subsurface-land surface-atmosphere feedbacks.

72 In this study, we applied TSMP over the European continent in predictive mode to assess the
73 evolution of water resources in the water year 2018/19 (September - August), the year after the
74 record-breaking drought 2018, focusing especially on the representation of atmospheric
75 uncertainty via ensemble simulations. The analyses concentrated on the Mid-European region
76 and included anomalies of atmospheric and hydrologic variables based on a previously generated
77 climatology. Additionally, we addressed the question whether the 2018 drought interacts with the
78 atmosphere and potentially reduces precipitation amounts in the water year 2018/19 causing a
79 positive drought feedback.

80 **2 Methods**

81 In the following, we briefly describe the relevant components of the integrated terrestrial systems
82 model applied in this study, the experimental setup of the probabilistic prediction system, and the
83 analyses of the anomalies and interactions with the atmosphere.

84 2.1 The Terrestrial Systems Modeling Platform (TSMP)

85 TSMP (Gasper et al., 2014; Shrestha et al., 2014) closes the terrestrial water and energy cycle
86 from groundwater across the land surface into the atmosphere coupling the atmospheric model
87 COSMO 5.1 with the land surface model CLM3.5 and the groundwater model ParFlow 3.2 via
88 the Ocean Atmosphere Sea Ice Soil Model Coupling Toolkit (OASIS3-MCT). Below, we
89 provide only a brief overview of TSMP; the interested reader is referred to Shrestha et al., 2014
90 and Gasper et al., 2014.

91 The non-hydrostatic model COSMO has been developed by a consortium of weather services
92 under the leadership of the German Weather Service (Baldauf et al., 2011). With different

93 configurations COSMO can serve as an operational weather forecast model or for regional scale
94 climate simulations. COSMO solves the primitive Euler-equations and includes multiple types of
95 precipitation, radiation and a 2.5 turbulence closure. It parametrizes shallow convection, energy
96 and momentum transfer with the surface.

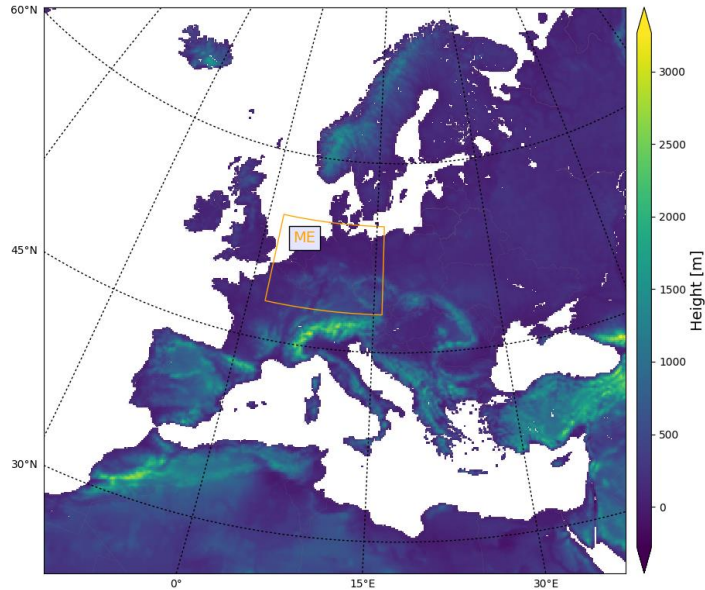
97 The Community Land Model (CLM3.5) consists of the shallow soil, snow layers, land cover,
98 vegetation and handles the interaction with the atmosphere (Oleson et al., 2004, 2008). To
99 accomplish this CLM3.5 parameterizes hydrologic, biologic and radiation processes, such as
100 evapotranspiration, sensible and ground heat. In TSMP, CLM3.5 supplies COSMO with the
101 boundary condition of surface albedos, energy fluxes, evapotranspiration, root-water uptake and
102 surface stresses. The land cover is described by sixteen different plant functional types (PFTs). In
103 TSMP, the hydrologic component of CLM3.5 is completely replaced by ParFlow.

104 The hydrological model ParFlow (Jones and Woodward, 2001; Ashby and Falgout, 1996; Kollet
105 and Maxwell, 2006; Maxwell, 2013) solves the 3D Richards equation with a Newton-Krylov
106 solver to model integrated variably saturated groundwater-surface water flow. In ParFlow,
107 Richards equation is discretized in space using finite differences and an implicit backward Euler
108 scheme in time. Overland flow is modeled by solving the kinematic wave equation in a finite
109 volume approach. ParFlow receives the incoming precipitation after canopy interception as well
110 as the water loss from evapotranspiration from CLM3.5. In turn, ParFlow provides the
111 hydrologic state to CLM3.5 in terms of soil moisture and matric potential.

112 In TSMP, the coupler OASIS3-MCT (Valcke, 2013) connects the different component models in
113 the form of independent executables based on a Multiple Process Multiple Data (MPMD)
114 approach. OASIS3-MCT acts as the driver initializing the models, managing the time steps and

115 coupling frequencies, exchanging the coupling data in 2-D arrays in memory and finally
116 terminating the simulation.

117 2.2 Model domain and setup



118

119 Figure 1. The European CORDEX model domain including the topographic height. The box
120 indicates the Mid-Europe (ME) focus region of this study.

121

122 The model domain shown in figure 1 has been implemented according to the Coordinated
123 Regional climate Downscaling Experiment (CORDEX) (Giorgi et al., 2009). The domain covers
124 all Europe based on a rotated latitude-longitude grid with a horizontal resolution of 0.11°
125 resulting in a resolution of approximately 12.5 km. COSMO has a vertical range of 50 km with a
126 time step of 60 s. CLM has ten soil layers ranging 3 m into the soil, ParFlow has five extra layers

127 covering in total 57 m depth below the land surface. The first ten layers of CLM and ParFlow are
128 identical. In ParFlow, there is a variable vertical discretization ranging from 2cm at the land
129 surface to more than $\sim 10^1$ m toward the bottom of the aquifer based on a terrain following grid.
130 CLM3.5 and ParFlow use a time step of 900 s, which also constitutes the coupling frequency.

131 Topographic slopes required by ParFlow were estimated from the USGS GTOPO30. Boundary
132 conditions on the coast are set by a constant hydraulic pressure with a hydrostatic profile for
133 ParFlow. The soil parameters of ParFlow model are estimated with the help of the Food and
134 Agricultural Organization (FAO) database (Carballas et al., 1990). To achieve this fifteen types
135 of soil are defined based on the texture information. To account for the loss of information due to
136 spatial aggregation and anisotropy, the values of the horizontal permeability are scaled by 1000.
137 For CLM, PFTs are obtained from the Moderate Resolution Imaging Spectroradiometer
138 (MODIS) database (Friedl et al., 2002). The individual values for stem and leaf area index and
139 the monthly bottom and top heights of the PFT are calculated with the global CLM surface data
140 set. Additional details of the setup can be obtained from Furusho et al., (2019)

141 2.3 Setup of the probabilistic prediction system

142 The setup of the probabilistic prediction system is directed at the goal to provide interannual
143 water resources predictions including droughts. The system is designed to account for the
144 climatologic atmospheric uncertainty, since atmospheric processes are arguably not predictable
145 at that time scale. To initialize the prediction, the terrestrial state in terms of water and energy at
146 the end of the previous water year was applied, in this case August 2018. This state was obtained
147 from a climatological/evaluation (EVAL) simulation starting in 1989 by Furusho et al. (2019)
148 based on atmospheric boundary conditions from ERA-Interim (Dee et al., 2011). Then the

149 following water year was simulated, here 2018/19, applying all previous years as atmospheric
 150 boundary conditions proposing that the predicted year is contained in the climatologic ensemble
 151 of all previous years with respect to atmospheric conditions. In this way, we are able to account
 152 for the climatologic atmospheric uncertainty without any prior assumptions. Furusho et al.
 153 (2019) analyzed the climatology starting from 1996 due to spin up effects that were detected in
 154 1989 to 1995. Therefore only the atmospheric forcing of the water years 1996 to 2018 was
 155 applied resulting in an ensemble of 22 forcing years for 2018/19 potentially reducing the real
 156 uncertainty range.

157 2.4 Analyses

158 In the analyses, we focused on the region of Mid-Europe (ME), where the drought 2018 was
 159 pronounced. For the analysis, the data was extracted in spatially averaged, monthly mean values.
 160 The variables considered at this point are 2m air temperature, tas (K), precipitation, pr (L), and
 161 total column water storage $s_{i,j}$ (L) from the land surface to the bottom of the aquifer. The latter
 162 constitutes an integrated measure of water resources and was calculated as follows

$$s_{i,j} = \sum_k^{nz} sat_{i,j,k} por_{i,j,k} dz_k$$

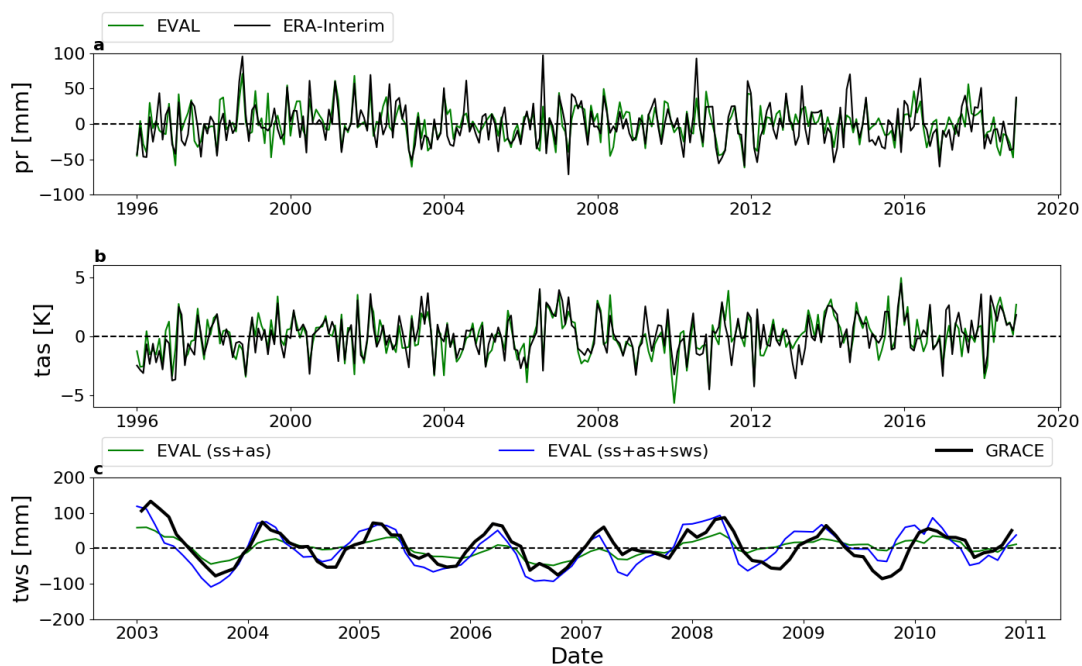
163 where $sat_{i,j,k}$ is the relative saturation (-), $por_{i,j,k}$ the porosity (-) for a pixel with indices i, j, k in
 164 the lateral and vertical direction, respectively, dz_k is the extent of a vertical grid cell (L) and nz is
 165 the number of grid cells in the vertical direction. This leads to a storage estimation for every
 166 subsurface column in the model. Utilizing the monthly mean values, monthly anomalies were
 167 calculated for each pixel and then the Mid-Europe (ME) domain.

168 In order to evaluate the simulations, ME averaged time series for *tas* and *pr* were compared to
169 ERA-Interim information, and *s* were compared to GRACE mascon data (Watkins et al., 2015).
170 In the latter, the *s* anomalies were recalculated based on the time period used in the GRACE
171 mascon data set. Interactions with the atmosphere were inspected, in particular precipitation, by
172 subtracting the monthly precipitation values from the probabilistic prediction. In other words,
173 every ensemble member of the year 2019 with the initial condition of the drought year 2018 was
174 subtracted from the corresponding values of the same month of EVAL. Box plots of precipitation
175 increments were generated for each month of the water year 2018/19 in order to identify
176 systematic changes in monthly precipitation amounts due to the dry initial condition in the
177 probabilistic predictions.

178 **4 Results and discussion**

179 While the probabilistic prediction covers all Europe, the 2018 drought was most pronounced in
 180 central, northern Europe. Therefore, in this study, we focus on Mid-Europe (ME), which is part
 181 of the PRUDENCE regions defined in Christensen and Christensen (2007).

182

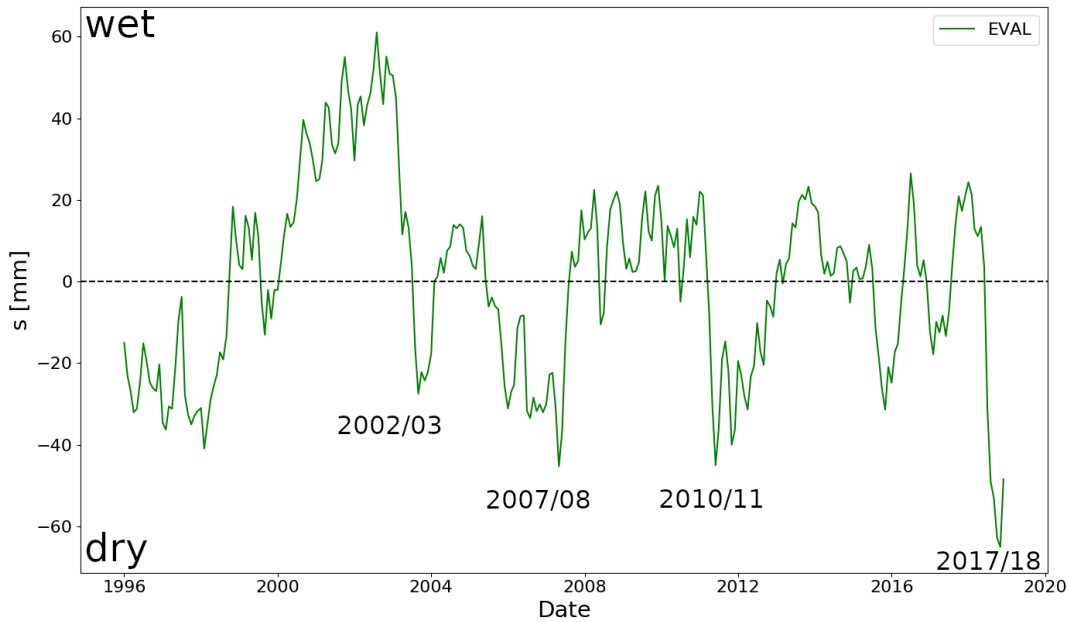


183

184 Figure 2. Anomalies calculated from ERA-Interim and the evaluation run, EVAL, from 1996 to
 185 2018 over Mid-Europe for (a) monthly precipitation, pr , and (b) air temperature, tas . Storage
 186 anomalies s (c) were calculated for the entire soil column including soil water, ss , and aquifer,
 187 as , storages ($ss + as$) and also surface water storage ($ss + as + sws$) based on the time period used
 188 on the GRACE mascon data set.

189

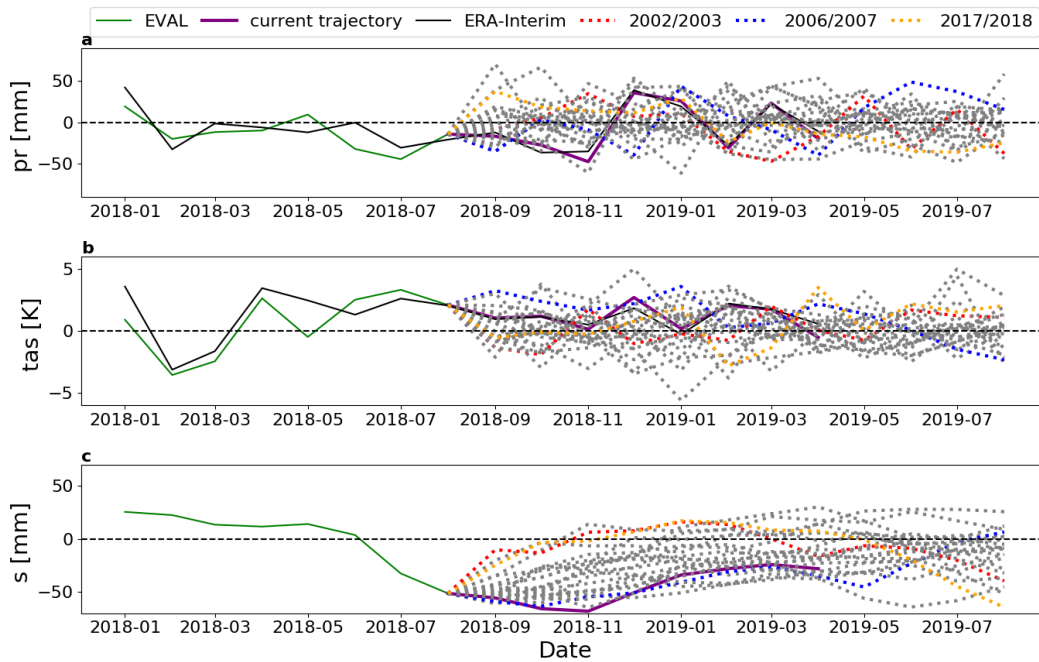
190 Figure 2 a) and b) show monthly anomalies of air temperature, tas and precipitation, pr ,
191 calculated over the subdomain ME from 1996 to 2018, respectively. The black curve shows
192 ERA-Interim for comparison. The plots for tas and pr anomalies show that the EVAL is in good
193 agreement with ERA-Interim, which is remarkable, because EVAL constitutes a transient
194 simulation without any correction (e.g. nudging). In case of s a comparison with the GRACE
195 mascon data was performed. In contrast to a) and b) the mean storage is calculated from 2004 to
196 2009 as a single value for the whole period to be comparable to the GRACE data. Additionally,
197 we derived two different water storage anomalies for EVAL. The first anomaly consists of soil
198 water storages, ss , and aquifer storage, as , following equation 1 covering the entire subsurface
199 column from the land surface to the bottom of the aquifer ($ss + as$). The second anomaly
200 additionally includes surface water of rivers and streams ($ss + as + sws$). There is a good
201 agreement with GRACE in case of subsurface and surface water storage anomalies ($ss + as +$
202 sws). In some years, there is a small phase shift in the simulated anomalies. Additionally the
203 anomalies in the water years 2007/08 and 2009/10 were over- and underestimated, respectively.
204 At this point, we explain these discrepancies with deviations of EVAL from real world
205 precipitation in these years. Additionally, snow and ice, and lakes were not included in the
206 anomalies from EVAL. The anomalies of subsurface storage ($ss + as$) only exhibit smaller
207 amplitudes and fewer dry anomalies, which is due to the inclusion of groundwater in the
208 analysis.



209

210 Figure 3. Time series of monthly column storage anomaly, s , averaged over Mid-Europe (ME)
 211 region.

212 Figure 3 shows the time series of monthly column storage anomalies averaged over the ME
 213 region. The major droughts of the water years 2002/03, 2007/08, 2010/11, and 2017/18 are
 214 clearly discernible. In addition, EVAL captures the transition from the extreme wet year of
 215 2001/02, which was characterized by the massive Elbe-Danube flood, to the extreme dry year
 216 2002/03 very well, which lends additional confidence in the forward simulations using TSMP.



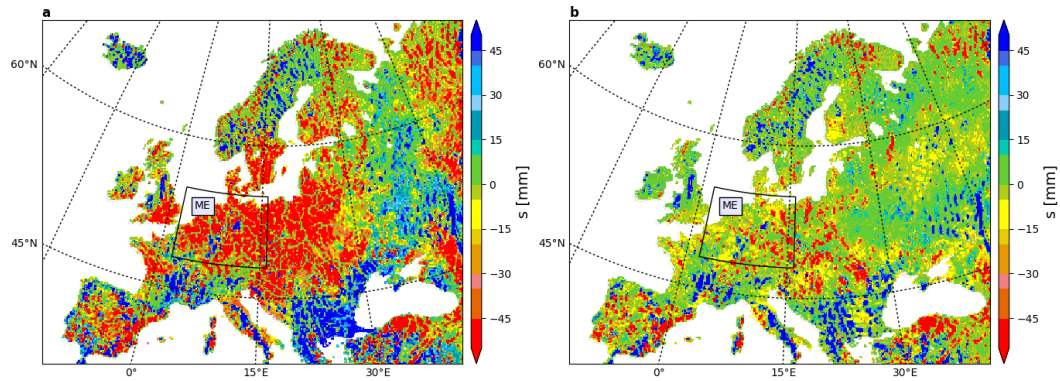
217

218 Figure 4. Plots of the period from the beginning of 2018 to August 2019 for the monthly (a)
 219 precipitation anomalies, (b) temperature anomalies and (c) the water storage anomalies. The
 220 probabilistic prediction period of the water 2018/19 includes all ensemble members in dashed
 221 lines and the current trajectory (purple solid line).

222

223 Figure 4 depicts the anomalies of pr , tas and s of EVAL for the period January until the end of
 224 August 2018 and the ensuing probabilistic prediction of the water year 2018/19. The heatwave is
 225 clearly visible with low precipitation (figure 4a) and high temperature anomalies (figure 4b).
 226 Over the course of the year, the influence of these two variables on the water storage, s , is
 227 apparent (figure 4c). The s anomaly changes from a wet (positive) anomaly to a strongly dry
 228 (negative) anomaly in August 2018. The hydrologic state at the end of August 2018 then served
 229 as the initial condition for the probabilistic forecast of 2019 based on the ensemble atmospheric

230 boundary conditions of 1996/97 to 2017/18. In figure 4c, the individual ensemble members are
231 plotted in dashed lines. We highlighted with colors dry forcing years that are 2002/03 and
232 2017/18, where the latter is a repetition of the extreme drought, and a wet year 2006/07.
233 Inspection of the ensemble member 2002/03 shows that, because the end of 2002 was rather wet,
234 this ensemble member is reducing the anomaly strongly, while the dry year 2003 increases again
235 the negative anomaly. A repetition of 2017/18 shows similar behavior resulting in an even
236 stronger deficit at the end of 2018/19. This is the only ensemble member that leads to an even
237 stronger dry anomaly at the end of the simulation. 2006/07 is a wet year in the ensemble that
238 turns the storage deficit into a positive anomaly. Most of the ensemble members reduce the dry
239 anomaly significantly until the summer 2019, however, the majority still exhibit a significant dry
240 anomaly at the end of the water year 2018/19. Thus, there is an increased probability that the
241 drought continues well into the water year 2019/20. Inspecting the current trajectory (purple line
242 in figure 4c) from the simulation using the most recent ERA-Interim boundary information (at
243 the time of submission) the dry anomaly is increasing even beyond the ensemble emphasizing
244 the strength of the drought 2018, which reached its peak in November 2018. While the dry
245 anomaly decreased during the winter and spring, the current trajectory is located in the dry tail of
246 the ensemble suggesting that there is a high probability of continuing drought conditions
247 throughout the current water year and potentially also 2019/20.



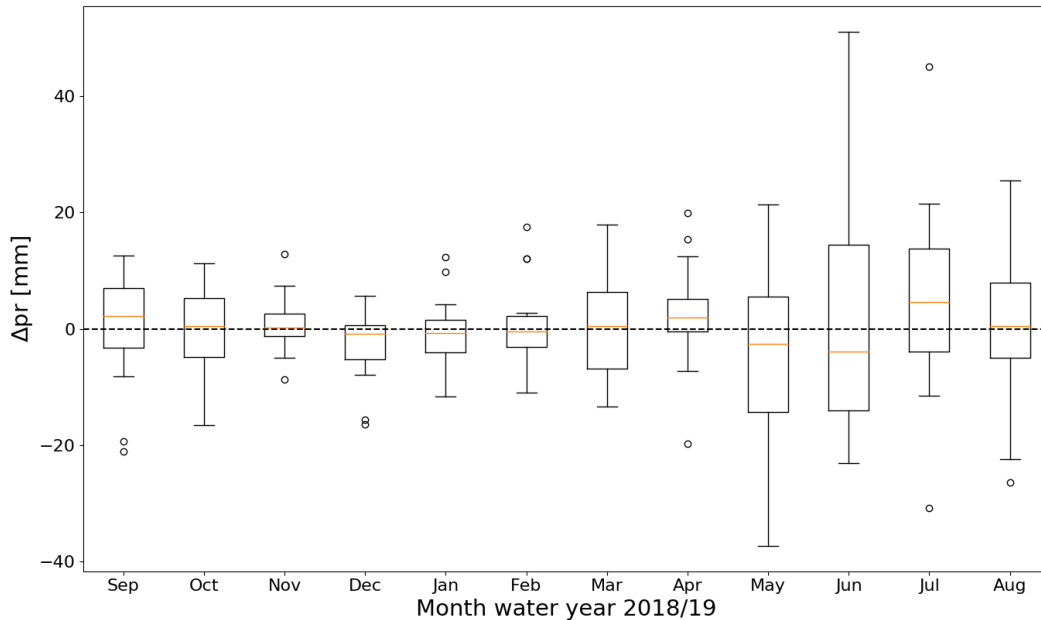
248

249 Figure 5. Water storage anomaly over the European model domain with a focus on the Mid-
 250 Europe region (ME) (a) for August 2018 and (b) the mean of all ensemble members in August
 251 2019.

252

253 Figure 5 provides the results of the spatial analyses of the s anomaly over Europe. In August
 254 2018 (figure 5a) the water deficit is significant, especially in the ME region, which is consistent
 255 with real-world observations. The ensemble mean (figure 5b) of the probabilistic prediction
 256 suggests that over large parts of ME the drought will persist at least until the end of the water
 257 year 2018/19. Figure 5 also emphasizes the strong spatial variability from the regional to the
 258 continental scale, which depends on multi-scale heterogeneity in physical parameters and fluxes
 259 especially related to evapotranspiration and precipitation. At the smallest spatial scale on the

260 order of the resolution of the model, the anomaly patterns need to be treated with care because of
 261 the uncertainty related to local rainfall amounts in the transient coupled simulations.



262

263 Figure 6. Boxplot of the difference of the evaluation run minus the corresponding ensemble
 264 member, Δpr , for all years. Lower to upper quartile are marked with the box, the median is
 265 indicated by the yellow line, the range of the data is indicated by the bars and the outliers are
 266 marked with circles.

267

268 The question remains, whether the extreme hydrologic drought interacted and continues to
 269 interact with atmospheric processes in the water year 2018/19. We attempted to answer the
 270 question in a rather *ad hoc* fashion at the spatial scale of the ME domain and the monthly time
 271 scale by inspecting the increments of monthly precipitation amounts from the individual

272 ensemble members and the years of the EVAL simulation. With the help of the increments we
273 tested the hypothesis that the extreme drought 2018 reduced precipitation amounts in the ensuing
274 water year 2018/19. Figure 6 shows the boxplots of the increments, which do not exhibit a
275 systematic reduction (or increase) in precipitation following the 2018 drought. The increments
276 fluctuate around zero with increasing variance until the end of the probabilistic prediction period,
277 which does not suggest a systematic reduction of precipitation amounts in the water year 2018/19
278 due to the drought 2018 at the considered space and time scale.

279 **5 Summary and conclusions**

280 The study proposes an interannual probabilistic prediction system of the terrestrial system from
281 groundwater across the land surface into the atmosphere at the continental scale. Atmospheric
282 uncertainty is accounted for by utilizing many years of historic atmospheric information as
283 boundary conditions for the predictions. The system was applied to the water year 2018/19 based
284 on the initial condition of the extreme drought at the end of the water year 2017/18 over the Mid-
285 -European region (ME), which is the focus of this study.

286 In order to verify the prediction system over ME, results from an extended evaluation simulation
287 from 1996 to 2018 were compared to results from ERA-Interim and GRACE satellite
288 information, which showed good agreement. While this lends confidence in the predictive skill
289 of the applied Terrestrial Systems Modeling Platform, additional verification is required for
290 additional variables, and different space and time scales. Further inspection of the evaluation
291 anomalies showed that 2018 was the strongest drought in terms subsurface water storage since
292 1996. The results from the probabilistic prediction indicated that there is a high probability of a
293 continuing water deficit at the end of August 2019 due to memory effects of the drought 2018 of

294 the subsurface-land surface system. The current trajectory of the water storage anomaly for
295 2018/19 suggests that the strong drought may persist also into 2019/20. Currently, 22 years of
296 historic atmospheric forcing has been applied in an attempt to capture the atmospheric
297 uncertainty, which is probably not enough. Additional years will be added to assess the
298 robustness of the approach. An increment analysis of precipitation amounts suggested that the
299 2018 drought did not influence precipitation in the water year 2018/2019 in an average sense
300 over ME. However the analysis was limited; in future, more work is needed to interrogate
301 subsurface-land and surface-atmosphere feedbacks across multiple space and time scales, and
302 variables. The prediction system has the potential to provide continues, quasi-operational
303 probabilistic predictions over the course of a water year given enough computational and data
304 storage resources, which are significant. Additionally, the current trajectory can be continuously
305 updated with incoming atmospheric re-analyses in order to provide continues information on the
306 current state of the terrestrial system. We provide this information and the data sets of this study
307 at https://datapub.fz-juelich.de/slts/prob_cordex/. Note, in this study, the system was applied in
308 the context of water scarcity. In the future, the potential for probabilistic flood forecasting will be
309 explored as well.

310 **Acknowledgments**

311 The authors gratefully acknowledge the computing time granted through JARA-HPC and the
312 VSR commission on the supercomputer JUWELS at Research Centre Jülich through compute
313 time projects cjibg35.

314 The work described in this paper has received funding from the Initiative and Networking Fund
315 of the Helmholtz Association (HGF) through the project “Advanced Earth System Modelling

316 Capacity (ESM)". The content of the paper is the sole responsibility of the author(s) and it does
317 not represent the opinion of the Helmholtz Association, and the Helmholtz Association is not
318 responsible for any use that might be made of the information contained. The data is made
319 available at https://datapub.fz-juelich.de/slts/prob_cordex/.

320 **References**

- 321 Ashby, S. F., & Falgout, R. D. (1996). A Parallel Multigrid Preconditioned Conjugate Gradient
322 Algorithm for Groundwater Flow Simulations. *Nuclear Science and Engineering*, 124(1),
323 145–159. <https://doi.org/10.13182/NSE96-A24230>
- 324 Baldauf, M., Seifert, A., Foerstner, J., Majewski, D., Raschendorfer, M., & Reinhardt, T. (2011).
325 Operational Convective-Scale Numerical Weather Prediction with the COSMO Model:
326 Description and Sensitivities. *MONTHLY WEATHER REVIEW*, 139(12), 3887–3905.
327 <https://doi.org/10.1175/MWR-D-10-05013.1>
- 328 Carballas, T., Macias, F., Diaz-Fierros, F., Carballas, M., & Fernandez-Urrutia, J. A. (1990).
329 FAO-UNESCO soil map of the world. Revised legend. *Informes Sobre Recursos Mundiales*
330 *de Suelos (FAO)*.
- 331 Christensen, J. H., & Christensen, O. B. (2007). A summary of the PRUDENCE model
332 projections of changes in European climate by the end of this century. *Climatic Change*,
333 81(SUPPL. 1), 7–30. <https://doi.org/10.1007/s10584-006-9210-7>
- 334 Dee, D. P., Uppala, S. M., Simmons, A. J., Berrisford, P., Poli, P., Kobayashi, S., et al. (2011).
335 The ERA-Interim reanalysis: Configuration and performance of the data assimilation
336 system. *Quarterly Journal of the Royal Meteorological Society*, 137(656), 553–597.
337 <https://doi.org/10.1002/qj.828>

- 338 Dirmeyer, P. A. (2000). Using a global soil wetness dataset to improve seasonal climate
339 simulation. *Journal of Climate*, 13(16), 2900–2922. [https://doi.org/10.1175/1520-](https://doi.org/10.1175/1520-0442(2000)013<2900:UAGSWD>2.0.CO;2)
340 [0442\(2000\)013<2900:UAGSWD>2.0.CO;2](https://doi.org/10.1175/1520-0442(2000)013<2900:UAGSWD>2.0.CO;2)
- 341 Friedl, M. A., McIver, D. K., Hodges, J. C. F., Zhang, X. Y., Muchoney, D., Strahler, A. H., et
342 al. (2002). Global land cover mapping from MODIS: Algorithms and early results. *Remote*
343 *Sensing of Environment*. [https://doi.org/10.1016/S0034-4257\(02\)00078-0](https://doi.org/10.1016/S0034-4257(02)00078-0)
- 344 Furusho, C., Goergen, K., Kulkarni, K., Keune, J., & Kollet, S. (2019). Pan-European
345 groundwater to atmosphere terrestrial systems climatology from a physically consistent
346 simulation. <https://doi.org/10.31223/OSF.IO/8VHG5>
- 347 Gasper, F., Goergen, K., Shrestha, P., Sulis, M., Rihani, J., Geimer, M., & Kollet, S. (2014).
348 Implementation and scaling of the fully coupled Terrestrial Systems Modeling Platform
349 (TerrSysMP v1.0) in a massively parallel supercomputing environment - a case study on
350 JUQUEEN (IBM Blue Gene/Q). *GEOSCIENTIFIC MODEL DEVELOPMENT*, 7(5),
351 2531–2543. <https://doi.org/10.5194/gmd-7-2531-2014>
- 352 Giorgi, F., Jones, C., Asrar, G. R., & others. (2009). Addressing climate information needs at the
353 regional level: the CORDEX framework. *World Meteorological Organization (WMO)*
354 *Bulletin*, 58(3), 175.
- 355 Hao, Z., AghaKouchak, A., Nakhjiri, N., & Farahmand, A. (2014). Global integrated drought
356 monitoring and prediction system. *Scientific Data*, 1, 140001.
357 <https://doi.org/10.1038/sdata.2014.1>

- 358 Hirschi, M., Seneviratne, S. I., Alexandrov, V., Boberg, F., Boroneant, C., Christensen, O. B., et
359 al. (2011). Observational evidence for soil-moisture impact on hot extremes in southeastern
360 Europe. *Nature Geoscience*, 4(1), 17–21. <https://doi.org/10.1038/ngeo1032>
- 361 Hosseini-Moghari, S. M., & Araghinejad, S. (2015). Monthly and seasonal drought forecasting
362 using statistical neural networks. *Environmental Earth Sciences*, 74(1), 397–412.
363 <https://doi.org/10.1007/s12665-015-4047-x>
- 364 Jones, J. E., & Woodward, C. S. (2001). Newton-Krylov-multigrid solvers for large-scale, highly
365 heterogeneous, variably saturated flow problems. *Advances in Water Resources*.
366 [https://doi.org/10.1016/S0309-1708\(00\)00075-0](https://doi.org/10.1016/S0309-1708(00)00075-0)
- 367 Keune, J., Gasper, F., Goergen, K., Hense, A., Shrestha, P., Sulis, M., & Kollet, S. (2016).
368 Studying the influence of groundwater representations on land surface-atmosphere
369 feedbacks during the European heat wave in 2003. *JOURNAL OF GEOPHYSICAL*
370 *RESEARCH-ATMOSPHERES*, 121(22), 13301–13325.
371 <https://doi.org/10.1002/2016JD025426>
- 372 Keune, J., Sulis, M., Kollet, S., Siebert, S., & Wada, Y. (2018). Human Water Use Impacts on
373 the Strength of the Continental Sink for Atmospheric Water. *GEOPHYSICAL RESEARCH*
374 *LETTERS*, 45(9), 4068–4076. <https://doi.org/10.1029/2018GL077621>
- 375 Kollet, S. J., & Maxwell, R. M. (2006). Integrated surface-groundwater flow modeling: A free-
376 surface overland flow boundary condition in a parallel groundwater flow model.
377 *ADVANCES IN WATER RESOURCES*, 29(7), 945–958.
378 <https://doi.org/10.1016/j.advwatres.2005.08.006>

- 379 Lo, M. H., & Famiglietti, J. S. (2010). Effect of water table dynamics on land surface hydrologic
380 memory. *Journal of Geophysical Research Atmospheres*, 115(22), 1–12.
381 <https://doi.org/10.1029/2010JD014191>
- 382 Madadgar, S., & Moradkhani, H. (2013). A Bayesian Framework for Probabilistic Seasonal
383 Drought Forecasting. *Journal of Hydrometeorology*, 14(6), 1685–1705.
384 <https://doi.org/10.1175/jhm-d-13-010.1>
- 385 Maxwell, R. M. (2013). A terrain-following grid transform and preconditioner for parallel, large-
386 scale, integrated hydrologic modeling. *Advances in Water Resources*, 53, 109–117.
387 <https://doi.org/10.1016/j.advwatres.2012.10.001>
- 388 Maxwell, R. M., Chow, F. K., & Kollet, S. J. (2007). The groundwater–land-surface–atmosphere
389 connection: Soil moisture effects on the atmospheric boundary layer in fully-coupled
390 simulations. *Advances in Water Resources*, 30(12), 2447–2466.
391 <https://doi.org/10.1016/J.ADVWATRES.2007.05.018>
- 392 Miguez-Macho, G., & Fan, Y. (2012). The role of groundwater in the Amazon water cycle: 1.
393 Influence on seasonal streamflow, flooding and wetlands. *Journal of Geophysical Research:*
394 *Atmospheres*, 117(D15), n/a-n/a. <https://doi.org/10.1029/2012JD017539>
- 395 Miralles, D. G., Gentine, P., Seneviratne, S. I., & Teuling, A. J. (2019). Land–atmospheric
396 feedbacks during droughts and heatwaves: state of the science and current challenges.
397 *Annals of the New York Academy of Sciences*, 1436(1), 19–35.
398 <https://doi.org/10.1111/nyas.13912>

- 399 Mishra, A. K., & Desai, V. R. (2005). Drought forecasting using stochastic models. *Stochastic*
400 *Environmental Research and Risk Assessment*, 19(5), 326–339.
401 <https://doi.org/10.1007/s00477-005-0238-4>
- 402 Oleson, K. W., Dai, Y., Bonan, G. B., Bosilovich, ., Dickinson, R. E., Dirmeyer, P. A., et al.
403 (2004). Technical Description of the Community Land Model (CLM). NCAR Technical
404 Note, NCAR/TN-46, 186. <https://doi.org/10.5065/D6N877R0>
- 405 Oleson, K. W., Niu, G. Y., Yang, Z. L., Lawrence, D. M., Thornton, P. E., Lawrence, P. J., et al.
406 (2008). Improvements to the community land model and their impact on the hydrological
407 cycle. *Journal of Geophysical Research: Biogeosciences*, 113(1).
408 <https://doi.org/10.1029/2007JG000563>
- 409 Rhee, J., & Im, J. (2017). Meteorological drought forecasting for ungauged areas based on
410 machine learning: Using long-range climate forecast and remote sensing data. *Agricultural*
411 *and Forest Meteorology*. <https://doi.org/10.1016/j.agrformet.2017.02.011>
- 412 Seneviratne, S. I., Corti, T., Davin, E. L., Hirschi, M., Jaeger, E. B., Lehner, I., et al. (2010).
413 Investigating soil moisture–climate interactions in a changing climate: A review. *Earth-*
414 *Science Reviews*, 99(3–4), 125–161. <https://doi.org/10.1016/J.EARSCIREV.2010.02.004>
- 415 Sheffield, J., Wood, E. F., Chaney, N., Guan, K., Sadri, S., Yuan, X., et al. (2013). A Drought
416 Monitoring and Forecasting System for Sub-Sahara African Water Resources and Food
417 Security. *Bulletin of the American Meteorological Society*, 95(6), 861–882.
418 <https://doi.org/10.1175/bams-d-12-00124.1>
- 419 Shrestha, P., Sulis, M., Masbou, M., Kollet, S., & Simmer, C. (2014). A Scale-Consistent
420 Terrestrial Systems Modeling Platform Based on COSMO, CLM, and ParFlow.

- 421 MONTHLY WEATHER REVIEW, 142(9), 3466–3483. <https://doi.org/10.1175/MWR-D->
422 14-00029.1
- 423 Valcke, S. (2013). The OASIS3 coupler: a European climate modelling community software.
424 Geoscientific Model Development, 6(2), 373–388. <https://doi.org/10.5194/gmd-6-373-2013>
- 425 Walko, R. L., Band, L. E., Baron, J., Kittel, T. G. F., Lammers, R., Lee, T. J., et al. (2000).
426 Coupled Atmosphere–Biophysics–Hydrology Models for Environmental Modeling. Journal
427 of Applied Meteorology, 39(6), 931–944. <https://doi.org/10.1175/1520->
428 0450(2000)039<0931:CABHMF>2.0.CO;2
- 429 Watkins, M. M., Wiese, D. N., Yuan, D.-N., Boening, C., & Landerer, F. W. (2015). Improved
430 methods for observing Earth’s time variable mass distribution with GRACE using spherical
431 cap mascons. Journal of Geophysical Research: Solid Earth, 120(4), 2648–2671.
432 <https://doi.org/10.1002/2014JB011547>
- 433 York, J. P., Person, M., Gutowski, W. J., & Winter, T. C. (2002). Putting aquifers into
434 atmospheric simulation models: an example from the Mill Creek Watershed, northeastern
435 Kansas. Advances in Water Resources, 25(2), 221–238. <https://doi.org/10.1016/S0309->
436 1708(01)00021-5
- 437 Yuan, X., & Wood, E. F. (2013). Multimodel seasonal forecasting of global drought onset.
438 Geophysical Research Letters, 40(18), 4900–4905. <https://doi.org/10.1002/grl.50949>
- 439 Yuan, X., Wood, E. F., Chaney, N. W., Sheffield, J., Kam, J., Liang, M., & Guan, K. (2013).
440 Probabilistic Seasonal Forecasting of African Drought by Dynamical Models. Journal of
441 Hydrometeorology, 14(6), 1706–1720. <https://doi.org/10.1175/JHM-D-13-054.1>

- 442 Zink, M., Pommerencke, J., Kumar, R., Thober, S., Samaniego, L., & Marx, A. (2016). The
443 German Drought Monitor. *Environmental Research Letters*, 17, 5625.